

Controllable Growth of Chains and Grids from Polyoxomolybdate Building Blocks Linked by Silver(I) Dimers

Hamera Abbas,^[a] Alexandra L. Pickering,^[a] De-Liang Long,^[a] Paul Kögerler,^[b] and Leroy Cronin^{*[a]}

Abstract: Molecular growth processes utilizing a β -octamolybdate synthon and $\{\text{Ag}_2\}$ dimers are described and the directing influence of “encapsulating” cations and coordinating solvent is also demonstrated. The growth of two 1D chains, $(n\text{Bu}_4\text{N})_{2n}[\text{Ag}_2\text{Mo}_8\text{O}_{26}]_n$ (**1**) and $(n\text{Bu}_4\text{N})_{2n}[\text{Ag}_2\text{Mo}_8\text{O}_{26}(\text{CH}_3\text{CN})_2]_n$ (**2**), is achieved when $n\text{Bu}_4\text{N}^+$ ions are used, and the diameter of the chains can be expanded by the coordination of CH_3CN solvent (**2**). The formation of a type of gridlike structure in which 1D chains are crossed-over each other in alternatively packed layers is achieved

in DMSO as the solvent; DMSO acts as a linking group to give $(n\text{Bu}_4\text{N})_{2n}[\text{Ag}_2\text{Mo}_8\text{O}_{26}(\text{dmsO})_2]_n$ (**3**), which, similar to **1** and **2**, still incorporates the Bu_4N^+ ions that exert an “encapsulating” influence. However, in $(\text{HDMF})_n[\text{Ag}_3(\text{Mo}_8\text{O}_{26})(\text{dmf})_4]_n$ (**4**) the relatively bulky Bu_4N^+ ions are exchanged for protonated DMF cations, thereby allowing the chains to con-

dense to a 2D array. The building block concept is further enforced by the isolation of a “monomeric” unit $(\text{Ph}_4\text{P})_2[\text{Ag}_2\text{Mo}_8\text{O}_{26}(\text{dmsO})_4]$ (**5**), which is isolated when the Ph_4P^+ ions are so “encapsulating” as to prevent aggregation of the $\{\text{Ag}-\text{Mo}_8-\text{Ag}\}$ building blocks. The nature of the $\text{Ag}\cdots\text{Ag}$ dimers in each of the compounds **1–4** is examined by DFT calculations and the interplay between these $\text{Ag}-\text{Ag}$ interactions and the structure types is described.

Keywords: density functional calculations · molybdenum · polyoxometalates · self-assembly · silver

Introduction

Polyoxometalate-based clusters represent a vast range of molecules based on aggregates of metal oxides of molybdenum,^[1] vanadium,^[1] and even niobium.^[2] Their versatile nature originates from the ability to polymerize metal-based polyhedra to form a range of clusters with low to high nuclearities ranging from 5 to 368 metal atoms in a single molecule.^[3] Polyoxometalate (POM) clusters have also been the subject of an immense number of studies, due to their attractive electronic and molecular properties that give rise to a variety of applications in many fields including catalysis,^[4] magnetism,^[5] medicinal chemistry,^[6] and materials science.^[7] Thus research towards understanding and manipulation of the self-assembly processes that underpin the formation of

POM clusters has to be an attractive route to enable the design of multifunctional materials, which take advantage of the unique physical properties associated with such clusters.^[8]

However, the most frequently found POM synthesis methods employ “one-pot” reactions to create structures of phenomenal diversity and with a wide range of nuclearities, and thus details on the complex formation mechanisms remain scarce and,^[1,3] as such, the manipulation of some of the many reaction parameters often represents a straightforward, but rather serendipitous, route to new POM architectures.^[1] One potential avenue of investigation that may allow the design of larger architectures based on clusters uses POM building blocks as synthons.^[9] This is because the ability to assemble large cluster systems from smaller known building blocks could be a direct way to systematically control the overall cluster architecture and properties, and thus might be the basis to work towards the growth of nanoscopic clusters of predetermined structure and function, a target that represents a fantastic challenge.

The major problem with this approach lies in establishing routes to produce reactive building blocks present in solution in significant concentrations and that can be reliably

[a] H. Abbas, A. L. Pickering, Dr. D.-L. Long, Dr. L. Cronin
Department of Chemistry
The University of Glasgow, Glasgow, G12 8QQ (UK)
Fax (+44) 141-330-4888
E-mail: L.Cronin@chem.gla.ac.uk

[b] Dr. P. Kögerler
Ames Laboratory and Department of Physics & Astronomy
Iowa State University, Ames, IA 50011 (USA)

utilized in the formation of larger architectures without reorganizing to other unknown fragments. Access to such building blocks has been the major limitation in stepwise growth of Mo-based POM clusters relative to the more kinetically inert W-based clusters, which have shown a degree of control; this is illustrated by the isolation of a $\{W_{148}\}$ cluster, which is a dodecamer of $\{XW_9\}$ units and four $\{W_5\}$ building blocks connected by lanthanide ions.^[10] Such limitations may be circumvented by adopting an approach that kinetically stabilizes the building block in solution, thereby effectively preventing its reorganization to other structure types.

Whilst developing strategies towards this goal, we recently reported a new family of polyoxomolybdates^[11] based on the $[H_2Mo_{16}O_{52}]^{10-}$ framework, which appears to achieve the first part of this goal, and allows the isolation of a new structure type by virtue of the cations used to “encapsulate” this unit, thereby limiting its reorganization to a simpler structure. Furthermore the building block character of this anion is demonstrated when electrophilic transition-metal ions M^{2+} ($M = Fe, Mn, Co$) are added to solutions of this cluster, resulting in $[H_2Mo_{16}M_2O_{52}]^{6-}$ species that can undergo further condensation reactions. These clusters were trapped by bulky organic cations during the self-assembly process and they appear to restrain the clusters from reorganizing into other well-known structure types. As an extension to this we have also trapped a family of sulfite-based Dawson-type mixed-valence polyoxomolybdates $[Mo_{18}O_{54}(SO_3)_2]^n-$ that possess unusual electronic properties and display unusual S...S interactions between the lone pairs of the two sulfite anions inside the cluster.^[12] Thus, the use of bulky organic cations in the formation of Mo-based POMs appears to restrict aggregation to the more highly symmetrical clusters, allowing a fundamentally more diverse set of clusters and cluster-based building blocks to be isolated that display unprecedented structural^[11] or physical^[12] features.

Here we report the successful extension of this “shrink-wrapping” strategy to the assembly of a diverse range of novel polymeric architectures based on the well-known β -octamolybdate $\beta-[Mo^VI_8O_{26}]^{4-}$ ion linked through coordination to electrophilic silver(I) ions. As such, these complexes represent rare examples of Ag-substituted POMs,^[13] and the use of such linkers to generate a family of polymeric polyoxomolybdate architectures is unprecedented. Further, the organic cations strongly influence the reactions by providing different degrees of encapsulation of the emerging inorganic polymer chains.

Results and Discussion

The dramatic effect of the use of encapsulating cations, here the tetra-*n*-butylammonium ion (nBu_4N^+), is demonstrated by the reaction of $(nBu_4N)_2[Mo_8O_{19}]$ with silver(I) fluoride in methanol; this reaction ultimately results in the formation of a unique one-dimensional chain structure of the composition:



In compound **1**, the flexible nBu_4N^+ ions nearly completely wrap around the linear chain of linked $[Ag^I Mo^VI_8O_{26}Ag^I]^{2-}$ units, see Figure 1. In the solid state^[14] (see Table 1 for crystallographic data), these strands are packed to a network of collinear, organic “tunnels” that accommodate the polymeric $\{Ag_2Mo_8\}_n$ (**1a**) anions. Within **1a**, each rhombohedral β -octamolybdate fragment, which consists of eight distorted, edge-sharing MoO_6 octahedra,^[15] contains fourteen terminal Mo=O groups. Eight of these form square O_4 arrangements ($O \cdots O = 3.013\text{--}3.157 \text{ \AA}$) that represent preferred, multidentate coordination sites for electrophilic metal centers. In **1a**, all octamolybdate fragments are identi-

Table 1. Crystallographic data for complexes **1–5**.

	1	2	3	4	5
empirical formula	$C_{32}H_{72}Ag_2Mo_8N_2O_{26}$	$C_{36}H_{78}Ag_2Mo_8N_4O_{26}$	$C_{36}H_{84}Ag_2Mo_8N_2O_{28}S_2$	$C_{15}H_{36}Ag_3Mo_8N_5O_{31}$	$C_{56}H_{64}Ag_2Mo_8O_{30}P_2S_4$
M_r [$g\ mol^{-1}$]	1884.18	1966.28	2040.43	1873.62	2390.51
crystal system	monoclinic	monoclinic	triclinic	triclinic	triclinic
space group	$P2_1/c$	$P2_1/n$	$P\bar{1}$	$P\bar{1}$	$P\bar{1}$
a [\AA]	9.7341(1)	10.4827(3)	12.9182(2)	9.9458(4)	11.2695(2)
b [\AA]	15.9359(4)	16.6484(4)	14.5922(3)	10.8856(3)	13.0331(2)
c [\AA]	17.5362(4)	16.8280(4)	16.9871(3)	11.7553(5)	14.0347(2)
α [$^\circ$]	90	90	76.988(1)	62.938(2)	92.615(1)
β [$^\circ$]	94.0421(11)	93.144(1)	86.366(1)	73.481(2)	98.527(1)
γ [$^\circ$]	90	90	83.784(1)	83.657(2)	114.193(1)
ρ_{calc} [$g\ cm^{-3}$]	2.306	2.227	2.187	2.864	2.150
V [\AA^3]	2713.45(10)	2932.41(13)	3099.07(10)	1086.31(7)	1846.55(5)
Z	2	2	2	1	1
$\mu(Mo_{K\alpha})$ [mm^{-1}]	2.556	2.381	2.323	3.644	2.065
T [K]	150(2)	150(2)	120(2)	150(2)	150(2)
reflns measured	44 448	22 362	49 689	15 718	27 303
independent reflns	7937	5754	12 158	4260	7255
observed reflns	7018	4829	10 878	3774	6755
parameters	316	345	746	290	461
$R1$ ($I > 2\sigma(I)$)	0.0235	0.0258	0.0289	0.0209	0.0233
$wR2$ (all data)	0.0556	0.0546	0.0698	0.0468	0.0595

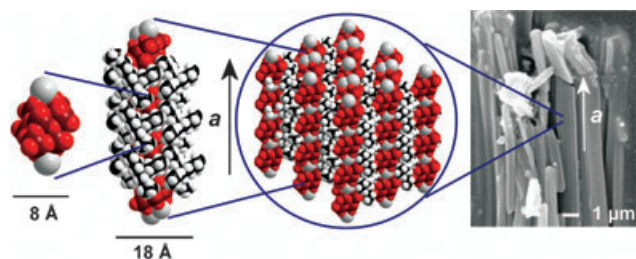


Figure 1. Space-filling representations of segments of the crystal structure of **1** containing the $\{\text{Ag}(\text{Mo}_8)\text{Ag}\}$ building block showing the growth of the structure into linear chains “shrink-wrapped” by the organic $n\text{Bu}_4\text{N}^+$ ions and the arrangement of the packed array of these chains (Mo: purple, O: red, Ag: gray, C: black, H: white). An SEM image of microcrystals of **1** is shown on the right with the crystallographic a axis parallel to the direction of the molecular chains.

cally oriented, whereby all O_4 groups are coplanar, face each other and are linked through two silver(i) centers. Each silver(i) center coordinates to two oxo positions of each O_4 group to form a virtually planar O_2AgO_2 bridging group, see Table 2. The Ag–O distances range from 2.2704(17) to 2.4143(15) Å, the O–Ag–O angles from 81.18(5) to 99.025(5)°. Interestingly, this silver(i) coordination mode results in close Ag–Ag contacts (2.8531(4) Å) that are shorter than metallic Ag⋯Ag distances, which suggests significant silver(i)–silver(i) interactions.^[16] The nature of the $\{\text{Ag}_2\}$ linker groups and the Ag coordination environments, however, were found to depend on the reaction conditions, which suggests that the precursors in the reaction solution are not individual $\{\text{Ag}_2\}$ and $\{\text{Mo}_8\}$ groups but, most probably, $\{\text{Ag}(\text{Mo}_8)\text{Ag}\}$ -type synthons.

Furthermore, the mode in which the $\{\text{Ag}(\text{Mo}_8)\text{Ag}\}$ -type “units” assemble to create the overall solid-state architecture was also found to be critically dependent on the reaction conditions. This is illustrated by the growth of radically different architectures, incorporating the same $\{\text{Ag}(\text{Mo}_8)\text{Ag}\}$ building block; modifications to the organic cation and solvent systems resulted in the isolation of polymeric compounds **2–4**:



Compounds **2–4** are analogues of **1** as they are based on linear chains of $\{\text{Ag}(\text{Mo}_8)\text{Ag}\}$ building blocks, and the formation of compounds **2** and **3** again is facilitated by the “shrink-wrapping” ability of the flexible $n\text{Bu}_4\text{N}^+$ ion. Additional ligands (**2**: acetonitrile, **3**: dimethylsulfoxide, **4**: *N,N*-dimethylformamide) are found to coordinate to all silver(i) centers in compounds **2–4**. In **2**, the $\{\text{Ag}_2\}$ bridging groups in the $\{\text{Ag}(\text{Mo}_8)\text{Ag}\}_n$ array are characterized by a shift in the Ag centers (relative to the situation found in **1**) so that each silver(i) ion has a terminal acetonitrile ligand and now caps one $\{\text{Mo}_8\}$ - O_4 group, that is, is coordinated in a tetradentate

fashion, and is linked to the neighboring $\{\text{Mo}_8\}$ fragment through one oxo position of the adjacent O_4 group, see Table 2. The $n\text{Bu}_4\text{N}^+$ counterions, although still surrounding the anionic polymer, are slightly displaced from the polymer (i.e., the channels incorporating the cluster strands in **2** are about 1.82 Å wider than in **1** due to the steric requirements of the acetonitrile ligands), see Figure 2.

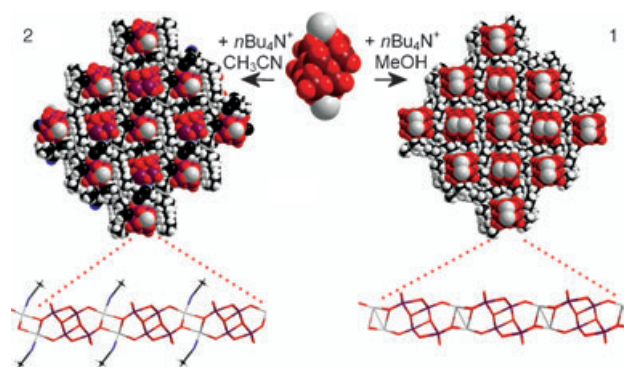
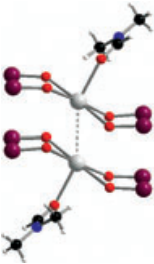
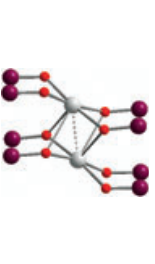
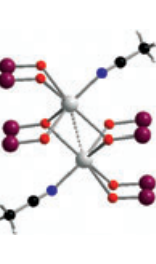
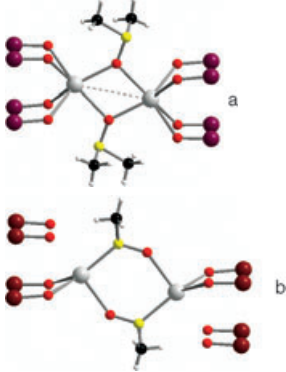


Figure 2. Space-filling packing representations, seen along the directions of the polymers, comparing the structures of compounds **1** and **2** and demonstrating the growth of the $\{\text{Ag}(\text{Mo}_8)\text{Ag}\}$ unit to one-dimensional **1** and **2**. Stick representations of each 1D chain are shown below in perpendicular views (Mo: purple, O: red, Ag: gray, C: black, N: blue, H: white).

Compound **3** is of special interest as it contains two types (a and b) of $\{\text{Ag}(\text{Mo}_8)\text{Ag}\}_n$ chains with different $\{\text{Ag}_2\}$ linking groups that cross-over in alternatively packed layers, whereby the angle between the chains of neighboring layers equates to approximately 86°, see Figure 3. In both types of chains the Ag positions do not directly bridge the $\{\text{Mo}_8\}$ groups, but each Ag center is coordinated to only one $\{\text{Mo}_8\}$ group. Neighboring Ag centers are then linked through two dimethylsulfoxide ligands to form $(\text{O}_4)\text{Ag}(\mu_2\text{-dmsO})_2\text{Ag}(\text{O}_4)$ bridges between the adjoining $\{\text{Mo}_8\}$ fragments. The two chain types differ in the bridging mode of the DMSO ligands: In the $\{\text{Ag}_2\}$ linker groups of a-type chains, both Ag positions coordinate to the μ -oxo centers of the DMSO molecules. The Ag– μ -O(SC_2H_6) distances are nearly equivalent (2.367/2.494 Å), resulting in an Ag⋯Ag distance of 3.8899(6) Å. In the b-type chains, the Ag⋯Ag distance is widened to 4.848(6) Å due to the bidentate bridging mode of the two DMSO- $\kappa\text{O},\kappa\text{S}$ molecules through both their oxygen and sulfur positions. In addition, while in a-type chains the Ag positions cap all four oxo positions of an O_4 group, the Ag centers in b-type chains coordinate to only two of the four oxo positions, see Table 2.

If the steric shielding ability of the “shrink-wrapping” organic cations is reduced, this “insulation” can partly be disrupted and the electrophilic polyoxomolybdate chains can be interlinked, illustrating the versatility of the “shrink-wrapping” concept as a strategy to new cluster-based networks. When for example, the $n\text{Bu}_4\text{N}^+$ ions in the reaction system are replaced with less bulky tetra-*n*-propylammonium ($n\text{Pr}_4\text{N}^+$) ions, compound **4** with a planar infinite grid

Table 2. Theoretical data for complexes **1–4**.^[a]

	4	1	2	3
coordination environment of {Ag ₂ } ^[b]				
Ag–O({Mo ₈ }) [average, Å]	2.413(3)	2.343(2) ^[c]	2.536(2)	a: 2.555(3) b: 2.375(3)
Ag...Ag [Å]	3.1475(6)	2.8531(4)	3.4543(6)	a: 3.8899(6) b: 4.848(6)
Ag–L [Å]	2.442(3) ^[d]	–	2.236(3) ^[e]	a: 2.366(3)/2.495(3) [O] b: 2.462(3) [S]/2.514(2) [O] ^[f]
partial Ag charge	0.123	0.144	0.089	a: 0.080, b: –0.03 ^[g]
Ag–Ag Mulliken overlap population	0.296	0.203	0.049	a: 0.046, b: 0.020
{Mo ₈ }...{Mo ₈ } [Å] ^[h]	6.835	6.644	7.509	a: 9.976, b: 11.612

[a] Comparison of the local Ag coordination environments in **1–4** and selected geometrical and electronic parameters. [b] Mo: purple, Ag: gray, O: red, C: black, H: white, N: blue, S: yellow. Ag–O contacts < 3.0 Å are shown. Ag...Ag contacts (< 4.0 Å) are represented by dotted gray lines. [c] Based on equatorial Ag–O bonds; the average including the long Ag–O bonds (2.835 and 2.913 Å) increases the average to 2.511 Å. [d] L = DMF. [e] L = MeCN. [f] L = DMSO. [g] Using the same basis sets and functionals, this net charge falls in the typical range (0.01 to –0.04) for discrete Ag⁺ complexes of oxo ligands, for example, the Ag⁺ positions in **5**. [h] Closest intrachain Mo...Mo distances between neighboring {Mo₈} groups.

structure of {Ag(Mo₈)Ag}_n strands results in the presence of *N,N*-dimethylformamide. In this case the employed *n*Pr₄N⁺ ions are *not* incorporated into the compound, but are replaced by protonated DMF (HDMF⁺) ions and additional silver(i) ions. Here, neighboring {Mo₈} fragments in each strand are linked by two Ag(dmf) groups that each bridge two oxo positions of an {Mo₈}-O₄ group, and in total connect two {Mo₈}-O₄ groups. Therefore each set of two oxo positions from the O₄ of neighboring {Mo₈}-O₄ groups together form two virtually planar {O₂AgO₂} bridging motifs similar to that in **1**, but resulting in a slightly larger Ag...Ag distance of 3.1475(6) Å, see Table 2. Due to the absence of “shrink-wrapping” *n*Bu₄N⁺ ions, additional [Ag(dmf)₂]⁺ ions now coordinate to terminal Mo=O groups perpendicular to the chain direction and interlink neighboring Y chains (closest interchain distance: 7.279 Å) through {Mo₈}-O₂-Ag(dmf)₂-O₂-{Mo₈} bridging motifs to form a planar 2D grid of parallel chains, see Figure 3.

Finally, the {Ag[Mo₈O₂₆]Ag} building block has been isolated by utilizing rigid, bulky tetraphenylphosphonium (Ph₄P⁺) ions that cannot facilitate chain growth by “shrink-wrapping” or adapting their conformation to promote {Ag(Mo₈)Ag}_n chain formation. In this case compound **5** is formed, which is composed of “monomeric” {Ag(Mo₈)Ag} anions, see Figure 4.

4.848(6) Å in **3** to 2.8531(4) Å in **1**. To probe the nature of the Ag...Ag contacts, comparative density functional theory (DFT) calculations were performed,^[15] the results of which indicate a significant bonding interaction between the Ag centers. Within the geometric boundaries of the series **1–4**, both the Mulliken overlap integrals and the atomic partial charges are primarily correlated with the coordination environment of the individual Ag positions and, to a lesser degree, the Ag...Ag distance. These parameters are summarized with the geometrical parameters of the Ag coordination environments in Table 2. In a first approximation, the findings can be explained by using a simple (electrostatic) crystal field model, according to which Ag(4d) electron density is repelled by the surrounding electronegative ligand positions and is stabilized between the Ag centers if significant Ag(4d)–Ag(4d) overlap is achieved; the partial atomic net charge correspondingly decreases with an increase in bonding overlap. Hence, the maximal Ag–Ag overlap and the minimal partial charges for Ag are observed for **4**, in which the Ag positions are ligated by {Mo₈}-oxo groups in a nearly square-planar geometry.

The coordination is completed by an apical DMF ligand that is *trans*-oriented to the neighboring Ag position ($\gamma(\text{O}(\text{dmf})-\text{Ag}-\text{Ag})=154^\circ$). Despite a shorter Ag...Ag contact and slightly lower average Ag–O({Mo₈}) distances, the

(Ph₄P)₂[Ag₂Mo₈O₂₆(dmsO)₄] **5**

The Ag centers here cap the two square O₄ faces of the β-[Mo₈O₂₆]⁴⁻ ion; the coordination environment of each Ag center is completed by the oxo positions of two terminal DMSO ligands (O–Ag–O angles ranging from 76.99(6) to 155.52(7)°, Ag–O distances from 2.355(2) to 2.624(2) Å). The isolation of molecular units in the crystal structure of **5** further emphasizes the crucial role of the *n*Bu₄N⁺ counterions in the formation of discrete infinite chains observed in **1–3**.

The molecular growth of the network architectures through the connection of β-{Mo₈}-based building blocks by silver(i) ions in the series **1–4** coincides with a gradual evolution of coordination modes of the silver(i) centers with respect to the relevant oxo ligands of the adjoined {Mo₈} fragments, exemplified by the shortening of the Ag...Ag distances within the {Ag₂} linker groups from

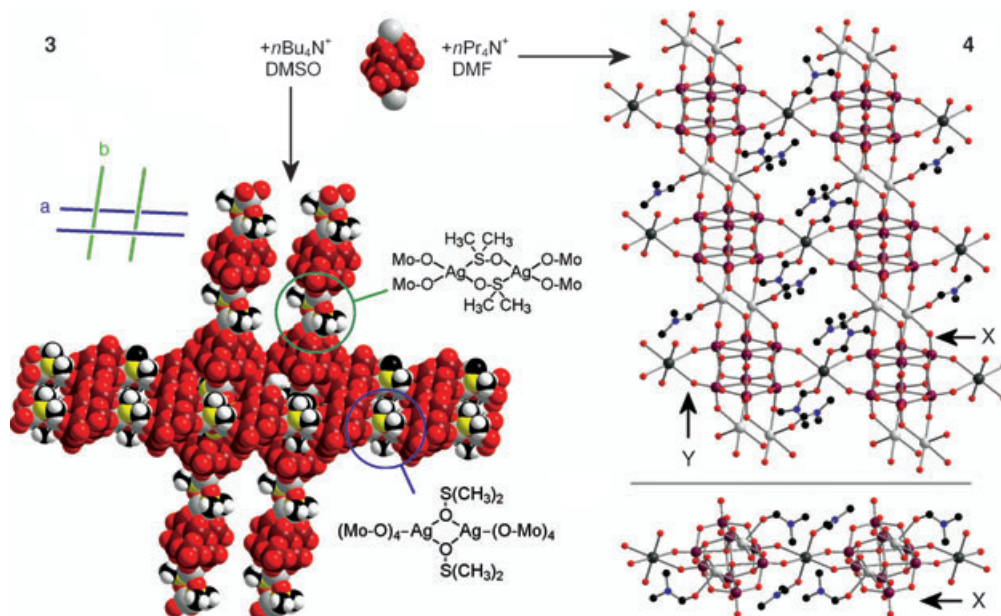


Figure 3. Left: CPK representation of a section of the layered grid structure of **3** based on two types (a and b) of linear $\{\text{Ag}(\text{Mo}_8)\text{Ag}\}_n$ chains. Two neighboring b-type chains of a central layer are shown sandwiched between two a-type chains of adjoining layers (as shown in the simplified scheme). To the right, the differences between the bridging $[\text{Ag}_2]$ groups (encircled) are emphasized. Right: Ball-and-stick representation of a section of the two-dimensional network **4** showing two connected strands X and Y (the arrows show the direction of the strands and strand X is shown isolated below for clarity). Above, parts of two $\{\text{Ag}(\text{Mo}_8)\text{Ag}\}_n$ chains are shown together with the Ag positions (dark gray) that coordinate to side-positioned terminal oxo positions of the $\{\text{Mo}_8\}$ fragments thus link the chains together. Below, the same section seen along the crystallographic *a* axis, illustrating the spatial arrangement of the DMF ligands. H positions are omitted (Mo: purple, O: red, Ag: gray, C: black, H: white, N: blue, S: yellow).

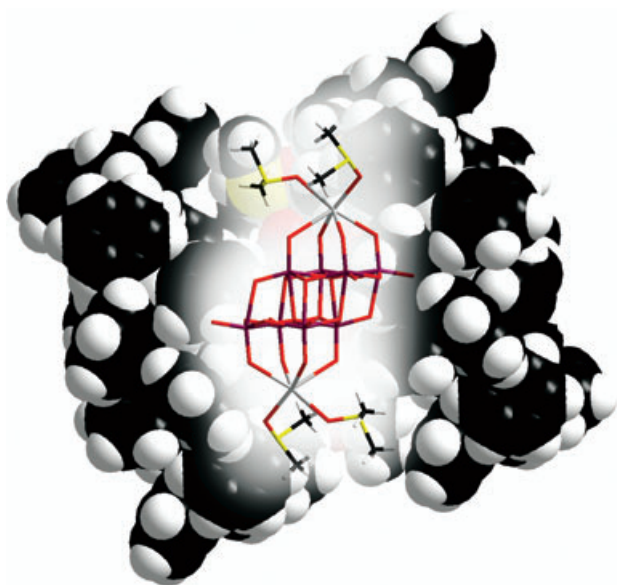


Figure 4. Representation of the structure of **5** shown in stick and space filling format (faded from center to the outside for clarity). The $[\text{Ag}_2\text{-Mo}_8\text{O}_{26}(\text{DMSO})_4]^{2-}$ cluster building block is shown surrounded by Ph_4P^+ ions which effectively isolate the whole cluster unit. (Mo: purple, Ag: gray, O: red, S: yellow, C: black, H: white).

Ag–Ag overlap is smaller for **1** due to the relative close distance of each Ag position to two oxo ligands of the neighboring Ag center (2.84 and 2.91 Å, respectively) and due to

the absence of a terminal ligand. In **2** the Ag–Ag overlap is further decreased, as the average Ag–O($\{\text{Mo}_8\}$) and the Ag...Ag distances widen. For **3** the Ag–Ag overlap and especially the partial charges decrease for both types of chains, most probably as a result of the large increase in the Ag...Ag distance.

Conclusion

This work demonstrates a strategy to control the molecular growth processes from $\{\text{Ag}(\text{Mo}_8)\text{Ag}\}^{2-}$ building blocks to linear molecular chains and grids, in which the choice of cation and solvent represents a crucial factor: the formation of the one-dimensional structures is directed by the flexible “shrink-wrapping” $n\text{Bu}_4\text{N}^+$ ion, whereas the larger, more rigid Ph_4P^+ ion along with capping DMSO ligands precludes the polymerization of the molecular building blocks. The smaller $n\text{Pr}_4\text{N}^+$ ion is replaced by additional silver(I) ions that are coordinated by the oxygen atoms located along the side of the cluster to link the polymer chains to a two-dimensional silver(I) coordination network. The gradual shortening of Ag...Ag distances from 4.848(6) and 3.8899(6) in **3**, 3.4543(6) in **2**, 3.1475(6) in **4**, and 2.8531(4) Å in **1** are caused by a gradual alignment of the $\{\text{Ag}(\text{Mo}_8)\text{Ag}\}$ building blocks and a concurrent change in electronic Ag–Ag interactions. Furthermore it is interesting that the $[\text{Mo}_6\text{O}_{19}]^{2-}$ ion can be used to reliably produce the $\beta\text{-}[\text{Mo}_8\text{O}_{26}]^{4-}$ synthon in solution, thereby allowing the development of a building

block strategy for the growth of architectures utilizing $\{\text{Ag}(\text{Mo}_8)\text{Ag}\}$ building blocks.^[17] Thus, these reactions represent examples for the control of the self-assembly processes of functional materials, which is of great interest in many areas of chemistry. Given the versatile electronic properties of POMs, these processes might become relevant for the production of spacers of specific dimensionality for use as a skeleton for conducting interconnectors in nanoscale electronic devices, or as e^- -beam resists. Future work will therefore concentrate on extending this molecular growth strategy to other POM-based structures, and to investigate their physical properties for potential applications.

Experimental Section

(Bu₄N)₂[Ag₂Mo₈O₂₆] (1): Silver(i) fluoride (28 mg, 0.22 mmol) in methanol (3 mL) was added to a solution of (Bu₄N)₂[Mo₆O₁₉] (150 mg, 0.11 mmol) in acetonitrile (4 mL). Filtration of the cloudy solution and diffusion of diethyl ether yielded colorless rectangular crystals over 2 days. Yield: 107 mg (0.057 mmol, 68%); elemental analysis calcd (%) for C₃₂H₇₂Ag₂Mo₈N₂O₂₆: C 20.39, H 3.85, N 1.48; found: C 20.53, H 3.78, N 1.53; IR (KBr): $\tilde{\nu}$ = 2960 (w), 2873 (w), 1481 (m), 1376 (w), 1153 (w), 1106 (w), 1025 (m), 952 (s), 921 (s), 890 (s), 8676 (s), 817 (s), 705 (s), 647 cm⁻¹ (m).

(Bu₄N)₂[Ag₂Mo₈O₂₆(CH₃CN)₂] (2): Silver(i) nitrate (19 mg, 0.11 mmol) in water (1 mL) was added to a solution of (Bu₄N)₂[Mo₆O₁₉] (75 mg, 0.055 mmol) in acetonitrile (5 mL) with trihydroxymethylaminomethane (13 mg, 0.11 mmol) and stirred for 4 h at room temperature. Filtration yielded a clear colorless solution from which colorless block crystals were obtained by evaporation over 24 h. Yield: 38 mg (0.019 mmol, 47%); elemental analysis for C₃₆H₇₈Ag₂Mo₈N₄O₂₆ showed decomposition to compound 1; IR (KBr): $\tilde{\nu}$ = 3433 (w), 2959 (s), 2872 (m), 1481 (s), 1378 (m), 870 (s), 821 cm⁻¹ (s).

(Bu₄N)₂[Ag₂(Mo₈O₂₆)(CH₃)₂SO]₂ (3): Silver(i) fluoride (3 mg, 0.024 mmol) in methanol (1 mL) was added dropwise to a solution of (Bu₄N)₂[Mo₆O₁₉] (75 mg, 0.055 mmol) in DMSO (3 mL) and stirred for 5 h at RT. Colorless block single crystals were obtained by diffusion of ethanol into the clear yellow solution over two weeks. Yield: 10 mg (0.005 mmol, 12%); elemental analysis calcd (%) for C₃₆H₈₄Ag₂Mo₈N₂O₂₆S₂: C 21.19, H 4.15, N 1.37; found: C 21.34, H 4.05, N 1.46; IR (KBr): $\tilde{\nu}$ = 3435 (m), 2961 (s), 2872 (s), 1633 (w), 1480 (s), 1378 (m), 1151 (w), 1003 (m), 943 (s), 835 cm⁻¹ (s).

(C₃H₈NO)[Ag₃(Mo₈O₂₆)(C₃H₇NO)₄] (4): Silver(i) nitrate (22 mg, 0.13 mmol) in methanol (3 mL) was added to a solution of (Pr₄N)₂[Mo₆O₁₉] (80 mg, 0.063 mmol) in DMF (6 mL) and stirred for 24 h at RT. Filtration yielded a clear yellow solution, from which colorless block crystals were obtained by diffusion of acetone over three weeks. Yield: 6 mg (0.003 mmol, 7%); elemental analysis calcd (%) for C₁₅H₃₆Ag₃Mo₈N₅O₃₁: C 9.62, H 1.94, N 3.74; found: C 9.84, H 2.00, N 3.28; IR (KBr): $\tilde{\nu}$ = 3427 (m), 2924 (m), 1648 (s), 1413 (w), 1382 (m), 1254 (w), 1101 (m), 942 (s), 902 (s), 841 cm⁻¹ (m).

(Ph₄P)₂[Ag₂Mo₈O₂₆(CH₃)₂SO]₄ (5): Silver(i) nitrate (22 mg, 0.13 mmol) in methanol (2 mL) was added to a solution of (Ph₄P)₂[Mo₆O₁₉] (100 mg, 0.06 mmol) in DMSO (5 mL) and stirred for 24 h at room temperature. Filtration yielded a clear, pale yellow solution, from which colorless block crystals were obtained by diffusion of diethyl ether over five days. Yield: 10 mg (0.004 mmol, 9%); elemental analysis calcd (%) for C₃₆H₆₄Ag₂Mo₈O₃₀P₂S₄: C 28.13, H 2.69; found: C 28.13, H 2.59; IR (KBr): $\tilde{\nu}$ = 3058 (w), 3014 (w), 1714 (m), 1481 (m), 1431 (s), 1402 (m), 1309 (m), 1166 (m), 1106 (s), 1012 (s), 933 (s), 910 (s), 887 (s), 831 (s), 759 cm⁻¹ (m).

X-ray crystallographic studies of the complexes: Data were measured at 150(2) K on a Nonius KappaCCD diffractometer ($\lambda(\text{MoK}\alpha) = 0.71073 \text{ \AA}$),

graphite monochromator. Structure solution was performed with the program SHELXS-97 and refinement with SHELXL-97.^[18] CCDC-248992-248996 contain the supplementary crystallographic data for this paper. These data can be obtained free of charge from The Cambridge Crystallographic Data Centre via www.ccdc.cam.ac.uk/data_request/cif.

Scanning electron microscope (SEM) measurements: Crystals of **1** were placed onto a copper substrate, and the sample was coated with gold. The SEM images were obtained by using a field emission SEM (JEOL, JSM-6400) operated at an acceleration voltage of 10 kV.

Computational studies: Density functional theory calculations (including Löwdin and Mulliken population analysis) were performed using the TURBOMOLE 5.6 package^[19] and required TZVP basis sets and B3-LYP hybrid functionals. Representative sections of the crystallographic coordinates were relaxed to converge, whereby maximal atomic shifts of 0.05 Å were observed.

Acknowledgement

This work was supported by the Leverhulme Trust (London), the Royal Society, the University of Glasgow, and the EPSRC. Ames Laboratory is operated for the U.S. Department of Energy by Iowa State University under Contract No. W-7405-Eng-82. We thank Dr. Jesus M. de la Fuente for help with the SEM measurements.

- [1] "High Nuclearity Polyoxometalate Clusters": L. Cronin, *Compr. Coord. Chem. II* **2004**, 7, 1.
- [2] M. Nyman, F. Bonhomme, T. M. Alam, M. A. Rodriguez, B. R. Cherry, J. L. Krumhansl, T. M. Nenoff, A. M. Sattler, *Science* **2002**, 297, 996.
- [3] A. Müller, E. Beckmann, H. Bögge, M. Schmidtman, A. Dress, *Angew. Chem.* **2002**, 114, 1210; *Angew. Chem. Int. Ed.* **2002**, 41, 1162.
- [4] I. V. Kozhevnikov, *Chem. Rev.* **1998**, 98, 171; J. T. Rhule, W. A. Neiwert, K. I. Hardcastle, B. T. Do, C. L. Hill, *J. Am. Chem. Soc.* **2001**, 123, 12101.
- [5] A. Müller, M. Luban, C. Schröder, R. Modler, P. Kögerler, M. Axenovich, J. Schnack, P. Canfield, S. Bud'ko, N. Harrison, *ChemPhys-Chem* **2001**, 2, 517; A. Müller, P. Kögerler, A. W. M. Dress, *Coord. Chem. Rev.* **2001**, 222, 193.
- [6] K. F. Aguey-Zinsou, P. V. Bernhardt, U. Kappler, A. G. Mcewan, *J. Am. Chem. Soc.* **2003**, 125, 530; D. A. Judd, J. H. Nettles, N. Nevins, J. P. Snyder, D. C. Liotta, J. Tang, J. Ermolieff, R. F. Schinazi, C. L. Hill, *J. Am. Chem. Soc.* **2001**, 123, 886;
- [7] H. D. Zeng, G. R. Newkome, C. L. Hill, *Angew. Chem.* **2000**, 112, 1842; *Angew. Chem. Int. Ed.* **2000**, 39, 1772; M. T. Pope, A. Müller, *Angew. Chem.* **1991**, 103, 56; *Angew. Chem. Int. Ed. Engl.* **1991**, 30, 34; F. Ogliaro, S. P. de Visser, S. Cohen, P. K. Sharma, S. Shaik, *J. Am. Chem. Soc.* **2002**, 124, 2806;
- [8] T. Yamase, *Chem. Rev.* **1998**, 98, 307.
- [9] A. Müller, P. Kögerler, C. Kuhlmann, *Chem. Commun.* **1999**, 1347.
- [10] K. Wassermann, M. H. Dickman, M. T. Pope, *Angew. Chem.* **1997**, 109, 1513; *Angew. Chem. Int. Ed. Engl.* **1997**, 36, 1445.
- [11] D.-L. Long, P. Kögerler, L. J. Farrugia, L. Cronin, *Angew. Chem.* **2003**, 115, 4312; *Angew. Chem. Int. Ed.* **2003**, 42, 4180; D.-L. Long, H. Abbas, P. Kögerler, L. Cronin, *J. Am. Chem. Soc.* **2004**, 126, 13880.
- [12] D.-L. Long, P. Kögerler, L. Cronin, *Angew. Chem.* **2004**, 116, 1853; *Angew. Chem. Int. Ed.* **2004**, 43, 1817.
- [13] R. Villanneau, A. Proust, F. Robert, P. Gouzerh, *Chem. Commun.* **1998**, 1491; J. T. Rhule, W. A. Neiwert, K. I. Hardcastle, B. T. Do, C. L. Hill, *J. Am. Chem. Soc.* **2001**, 123, 12101.
- [14] After the submission of this work for publication, the structure of compound **1** was reported see S.-M. Chen, C.-Z. Lu, Y.-Q. Yu, Q.-Z. Zhang, H. He, *Inorg. Chem. Commun.* **2004**, 7, 104. Although both structures are essentially identical, our residuals are approximately

- 50% smaller and our unit cell is slightly compressed, presumably because our data was collected at 150 K versus room temperature for this work.
- [15] U. Lee, H.-C. Joo, M.-A. Chob, *Acta Crystallogr. Sect. E* **2002**, 58, 599; Q. Wang, X. Xu, X. Wang, *Acta Crystallogr. Sect. C* **1993**, C49, 464.
- [16] M. Jansen, *Angew. Chem.* **1987**, 99, 1136; *Angew. Chem. Int. Ed. Engl.* **1987**, 26, 1098.
- [17] Y. Wei, B. Xu, C. L. Barnes, Z. Peng, *J. Am. Chem. Soc.* **2001**, 123, 4083.
- [18] Structure solution with SHELXS97 and refinement with SHELXL97 using WinGX: L. J. J. Farrugia, *Appl. Crystallogr.* **1999**, 32, 837.
- [19] O. Treutler, R. Ahlrichs, *J. Chem. Phys.* **1995**, 102, 346.

Received: August 30, 2004
Revised: October 28, 2004
Published online: ■ ■ ■, 2005